

Identity Preserving 3D Head Stylization with Multiview Score Distillation

Bahri Batuhan Bilecen Ahmet Berke Gokmen Furkan Guzelant Aysegul Dunder
 Bilkent University, Department of Computer Engineering
 Ankara, Türkiye

{batuhan.bilecen@, berke.gokmen@ug, furkan.guzelant@, adundar@cs}.bilkent.edu.tr

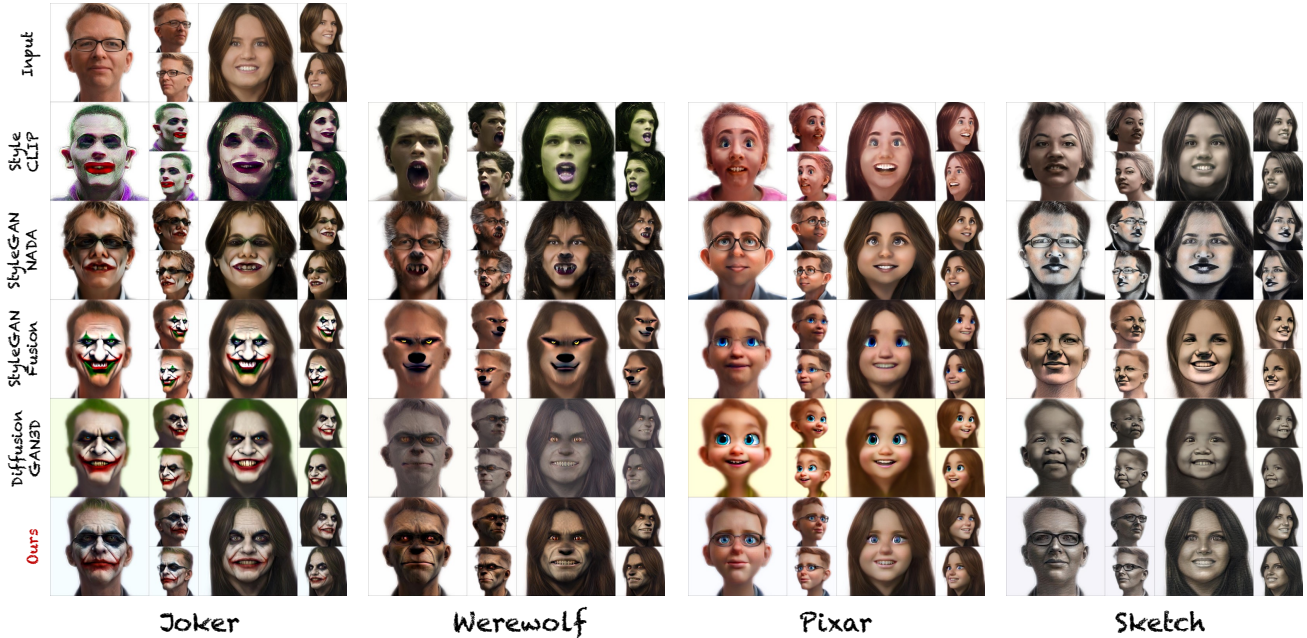


Figure 1. Our method effectively balances stylization and identity preservation, whereas other approaches often struggle to achieve high-quality stylization and accurate identity retention. Notably, other methods generate identical faces for different inputs (e.g., Joker stylization), whereas ours preserves unique features for each input, ensuring distinct and personalized results for every individual face.

Abstract

3D head stylization transforms realistic facial features into artistic representations, enhancing user engagement across applications such as gaming and virtual reality. While 3D-aware generators have made significant advancements, many 3D stylization methods primarily provide near-frontal views and struggle to preserve the unique identities of original subjects, often resulting in outputs that lack diversity and individuality. This paper addresses these challenges by leveraging the PanoHead model, synthesizing images from a comprehensive 360-degree perspective. We propose a novel framework that employs negative log-likelihood distillation (LD) to enhance identity preservation and improve stylization quality. By integrating multi-view grid score and mirror gradients within the 3D GAN architecture and introducing a score rank weighing technique, our approach

achieves substantial qualitative and quantitative improvements. Our findings not only advance the state of 3D head stylization but also provide valuable insights into effective distillation processes between diffusion models and GANs, focusing on the critical issue of identity preservation. Please visit the [project page](#).

1. Introduction

3D head stylization refers to transforming realistic facial and head features into artistic representations that can be rendered from multiple viewpoints, providing a dynamic and immersive experience. 3D head stylization has diverse applications in entertainment, advertising, education, enhancing user engagement, and creating relatable characters, and it is also a popular research topic due to its potential for

innovation and impact across various fields.

Previously, face stylization was extensively explored in 2D image domains [13, 40, 43, 56], particularly through generative models like StyleGAN [24], which allowed for the manipulation of stylistic elements to create diverse, high-quality facial representations. With recent advancements in realistic 3D-aware face generators [4, 8], research in stylization has now shifted to the 3D domain [1, 5, 25, 26, 29, 50, 51, 61], as these models enable the creation of lifelike representations that can be viewed from multiple angles, significantly enhancing user experiences in applications such as gaming, virtual reality, and animation.

Most of these methods proposed for 3D stylization are built on the EG3D generator [8], which primarily synthesizes near-frontal views. This limitation restricts the generation of comprehensive 3D scenes from diverse viewpoints. In this work, we focus on PanoHead [4], which excels in synthesizing images from a 360-degree perspective. We establish applicable baselines using PanoHead, highlighting the challenges of stylizing 360-degree heads. Our findings demonstrate that most of the current methods fall short of effectively achieving comprehensive and cohesive stylization across all angles. This limitation arises because many of these methods rely on stylized images that are primarily available in near-frontal views that fine-tuned StyleGAN models generate [1, 50, 61].

There are other works that leverage text-based image diffusion or CLIP models to either generate datasets or guide training [5, 25, 26, 29, 51] providing more flexibility, especially for 3D generators. Especially, the Score Distillation Sampling (SDS) algorithm [45] has demonstrated its effectiveness in providing sufficient training feedback for the stylization of 3D portraits [29, 51]. It leverages the insights from text-based diffusion models to propagate signals through backpropagation. However, it has been noted that the SDS technique can result in a loss of diversity in the generated outputs [29]. For example, when the generator is fine-tuned for a Joker or Pixar style, the outputs from random samplings tend to exhibit significant similarity. Even though DiffusionGAN3D [29] introduces a relative distance loss to mitigate diversity loss, we find that its outputs, along with those from other competing methods, tend to be similar for different inputs. This results in challenges with identity preservation, as illustrated in Fig. 1. The outputs tend to be similar across different inputs, resulting in a loss of the unique identity of the original images.

Based on this observation, we propose a framework that achieves 3D head stylization with identity preservation in this work. Specifically,

- We propose using distillation with negative log-likelihood distillation (LD) [20] for domain adaptation of 3D-aware image generators, yielding sharper and more ID-preserving results compared to SDS [45].

- We propose **rank weighing for score tensors** on latent channels to regularize the LD gradients, which we show achieve better input color and ID preservation in the distillation process.
- In compliance with the 3D GAN architecture [4], we extend LD with **multi-view grid and mirror score gradients** for improved stylization quality. Noting the importance of super-resolution (SR) networks in style-based GANs in domain adaptation, we avoid distilling grid scores to SR layers to further improve stylization.

Our method has shown significant qualitative and quantitative improvements over the relevant head stylization methods and provides important insights into the distillation from diffusion to GAN backbones.

2. Related Work

3D-aware generators. Generative Adversarial Networks (GANs), when integrated with differentiable renderers, have made significant advancements in generating 3D-aware images consistent across multiple views. While earlier methods focus on mesh representations [11, 12, 15, 41], the latest innovations leverage implicit representations [9, 14, 36, 39]. Among implicit representations, triplane representations have become particularly popular due to their computational efficiency and the high quality of the generated outputs [4, 8]. The architectures of models like EG3D [8] and PanoHead [4] are reminiscent of the StyleGAN2 structure [24]. These frameworks consist of mapping and synthesis networks that create triplanes, which are then projected into 2D images through volumetric rendering processes similar to those used in NeRF [34]. While EG3D is trained on the FFHQ dataset [23] with limited angle diversity, PanoHead allows for a 360-degree perspective in face generation, attributed to its dataset selection and model enhancements. In our work, we investigate PanoHead to achieve 3D portrait stylization. We are interested in 3D portrait stylization of real input images, which requires embedding images into PanoHead’s latent space. This task is referred to as image inversion and extensively studied for StyleGAN generators [2, 3, 42, 46, 58, 59] and recently for 3D-aware GAN models [6, 7, 30, 54, 60].

Adopting image generators to new domains. A popular method for stylizing 2D and 3D portraits involves fine-tuning generators initially trained to produce realistic faces. This process, known as domain adaptation of generators, utilizes the generators’ expertise in synthesizing real images. It can be accomplished using either a small number of samples for each style [31, 37] or by employing text-guided models to direct the training process [5, 25, 26, 29, 51]. Using text-based models to guide stylization offers the advantage of generating styles based on various prompts, which can be challenging to sample directly. These models, trained on extensive datasets, effectively acquire knowl-

edge in a disentangled manner, enabling them to produce meaningful results for intriguing prompts that may not have corresponding data available [38, 44, 48]. Moreover, this guidance can be provided from multiple poses for 3D-aware generators, allowing for flexibility beyond the poses in the collected datasets. While previously, CLIP loss has been a popular choice for the guidance [19, 35, 49], more recently, the Score Distillation Sampling (SDS) algorithm has demonstrated impressive performance [29, 45, 51]. However, previous research indicates that when generators are fine-tuned solely using SDS losses, they may collapse into producing a fixed image pattern, irrespective of the input noise [29, 51]. To promote diversity, both StyleGANFusion [51] and DiffusionGAN3D [29] introduce regularizers aimed at enhancing variety. However, we observe that this diversity remains constrained, leading to issues with identity preservation, where different inputs yield similar outputs. In this work, we propose a framework that enables 3D portrait stylization guided by text prompts while maintaining identity preservation.

3. Method

Our method involves fine-tuning the pre-trained parameters of PanoHead to adapt it for generating images from different domains. This section will go through the development of the method. Specifically, we will explain the adoption of LD to 3D-aware image generators, mention the differences between SDS, extend LD with cross-pose dependencies and grid denoising, and use rank reduction on score tensors.

3.1. Preliminaries

Denoising diffusion probabilistic models (DDPM). In the forward process of DDPM [17], Gaussian noise ϵ is gradually added to the initial data point x_0 over time steps t , reaching a pure Gaussian \mathcal{N} as $t \rightarrow T$ (Eq. (1)). Since we use a latent diffusion model [47], we denote image latent vectors with x for simplicity. In the reverse process, the denoising UNet $\hat{\epsilon}$ is trained to predict the noise ϵ added at each time step t with the MSE objective (Eq. (2)).

$$\sqrt{\bar{\alpha}_t}x_0 + \sqrt{1 - \bar{\alpha}_t}\epsilon = x_t, \quad \epsilon \sim \mathcal{N}(0, \mathbf{I}) \quad (1)$$

$$\mathbb{E}_{x_0, \epsilon, t} \{ \|\epsilon - \hat{\epsilon}(x_t, t)\|^2 \} \quad (2)$$

Score-based stochastic differential equations (SDE). In the score-based SDE framework [52], the forward process (Eq. (3)) adds Gaussian noise to x over time, where $g(t) = \sqrt{1 - \bar{\alpha}_t}$ is the noise scale and w is Wiener process. The reverse process (Eq. (4)) is modeled as a reverse-time SDE and denoises x by moving in the direction of higher probability density, where $\nabla_{x_t} \log p(x|y)$ is the *score function*. We keep the drift terms $f = 0$ for simpler notation.

$$dx = g(t)dw \quad (3)$$

$$dx = -g(t)^2 \nabla_{x_t} \log p(x|y)dt + g(t)d\bar{w} \quad (4)$$

The relation between the score function and the noise prediction can be described in Eq. (5):

$$\nabla_{x_t} \log p(x|y) \approx \frac{-\hat{\epsilon}(x_t, t|y)}{g(t)} \quad (5)$$

PanoHead. PanoHead [4] generates hybrid 3D representations called *triplanes* with a StyleGAN-like architecture which takes 512-dimensional style vectors and outputs 256×256 resolution triplanes. These triplanes are rendered from a specified camera pose using a neural volumetric renderer to synthesize a 2D head image with size 64×64 . Finally, a convolution-based super-resolution (SR) network performs upscaling from 64×64 images to 512×512 final images to refine details. Since the SR network upscales significantly, it plays a critical role in maintaining geometric consistency while prioritizing a rich texture and color.

3.2. ID-Preserving Stylization with Distillation

Likelihood distillation (LD) objective. We adopt a part of the distillation procedure in [20] explained in this section briefly. A detailed derivation is provided in Supplementary for completeness.

Assume that distribution (q) of the 3D representation (θ) conditioned on text prompt (y) is proportional to the prompt-conditioned distribution (p) of independent 2D renders (x_0^i) on different poses (i):

$$q(\theta|y) \propto p(x_0^0, x_0^1, \dots, x_0^N|y) = \prod_i^N p(x_0^i|y) \quad (6)$$

We optimize negative log-likelihood of Eq. (6) to find θ :

$$-\log q(\theta|y) = -\log \prod_i^N p(x_0^i|y) = -\sum_i^N \log p(x_0^i|y) \quad (7)$$

Define the loss \mathcal{L}_{LD} and find gradient ∇_{θ} to update θ via gradient descent:

$$\nabla_{\theta} \mathcal{L}_{LD} = -\mathbb{E}_{\pi} \{ \nabla_{\theta} \log p(x_0^{\pi}|y) \} \quad (8)$$

Combining Eqs. (1) and (8) results in:

$$\nabla_{\theta} \log p(x_0^{\pi}|y) = \nabla_{x_t} \log p(x_t^{\pi}|y) \frac{\partial x_t^{\pi}}{\partial x_0^{\pi}} \frac{\partial x_0^{\pi}}{\partial \theta} \quad (9)$$

where $\nabla_{x_t} \log p(x_t^{\pi}|y)$ is the score function estimation. Plugging Eq. (9) into Eq. (8) yields the update direction:

$$\nabla_{\theta} \mathcal{L}_{LD} = -\mathbb{E}_{\pi, x_t} \left\{ \nabla_{x_t} \log p(x_t^{\pi}|y) \frac{\partial x_t^{\pi}}{\partial x_0^{\pi}} \frac{\partial x_0^{\pi}}{\partial \theta} \right\} \quad (10)$$

where $\frac{\partial x_t^{\pi}}{\partial x_0^{\pi}}$ is $\sqrt{\bar{\alpha}_t}$ from Eq. (1). Notice that to update θ , we do not need to back-propagate through the denoiser and

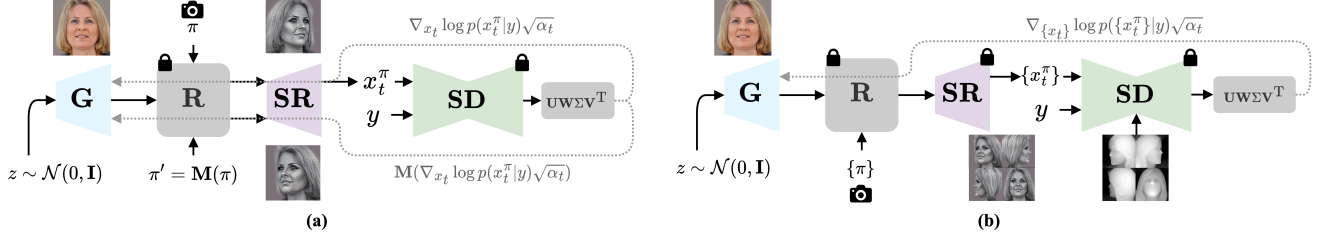


Figure 2. Our proposed training approach with mirror gradients (a) and grid distillation (b). Dashed and non-dashed lines show backpropagation and forward paths. G , R , SR , and SD denote generator, neural renderer, super-resolver, and denoising UNet, respectively. Output of SD is the score, $\nabla_{x_t} \log p(x_t^\pi | y)$. We employ a depth-conditioned ControlNet in (b).

can acknowledge the output as a part of the gradient. For the domain adaptation task, we assign θ as the PanoHead layers.

Note that LD is different than SDS [45] as it optimizes negative log-likelihood instead of reverse KL-divergence. Compliant with previous observations [53], we also observe that SDS yields blurry results, as LD is sharp in domain adaptation tasks. We attribute this to the fact that SDS is inherently mode-seeking due to the subtraction of ground truth noise ϵ from the estimated noise $\hat{\epsilon}$ and high classifier free guidance (CFG) [18] weight to avoid divergence [45]. In comparison, LD is diversity-seeking by not utilizing ϵ , and does not require very high CFG weights, promoting diversity among samples.

We also note that even though LD yields sharper results, it is also said to suffer from stability in longer training regimes; hence, a balanced score distillation approach on top of Eq. (10) is proposed [20]. However, we observe that the strong prior of the GAN backbone is enough to avoid divergence with LD.

Rank weighted score tensors. While LD reduces the smoothness issues, we come across some artifacted results, especially around the hair, ears, and neck on some prompts (Fig. 3, full-rank). Notice that the artifacts are more focused on incorrect color distribution rather than the style itself. Inspired by previous work utilizing feature decomposition techniques [21, 27] and expecting a disentanglement, we investigate the SVD of the score tensors along the VQ-VAE latent channel (4) dimension. We notice that the first rank contains most of the stylization and conclude that surpassing the contributions of the lower three ranks can mitigate undesired tints. Hence, we re-weigh the diagonal singular value matrix \mathbf{S} with linearly decaying coefficients \mathbf{W} from the largest singular value to the smallest. Specifically,

$$\begin{aligned} \mathbf{U}\Sigma\mathbf{V}^T &= \text{SVD}(\nabla_\theta \log p(x_0^\pi | y)) \\ \nabla_\theta \log \tilde{p}(x_0^\pi | y) &= \mathbf{U}\mathbf{W}\Sigma\mathbf{V}^T \end{aligned} \quad (11)$$

\tilde{p} is the rank-weighted score distribution, $\Sigma_{4 \times 4} = \text{diag}(\sigma_1, \sigma_2, \dots, \sigma_4)$, $\mathbf{U}_{4 \times 4} = [u_1, u_2, \dots, u_4]$, $\mathbf{V}_{4096 \times 4} = [v_1, v_2, \dots, v_4]$, and $\mathbf{W} = \text{diag}(1, 0.75, 0.5, 0.25)$.

As seen in Fig. 3, rank-weighted score tensors eliminate the problematic tints and set a good baseline for the following improvements. We set the weight scores based on our empirical analysis, and the same weights are used for the training of all prompts.

Extending LD via cross-dependencies with mirror poses. The expression in Eq. (10) does not consider the correlation between different views. To add cross-dependencies, we account for another poses where $\pi' \neq \pi$ in Eq. (12):

$$\begin{aligned} \nabla_\theta \mathcal{L}_{LD} &= -\mathbb{E}_{\pi, x_t} \left\{ \nabla_{x_t} \log p(x_t^\pi | y) \frac{\partial x_t^\pi}{\partial x_0^\pi} \frac{\partial x_0^\pi}{\partial \theta} \right. \\ &\quad \left. + \sum_{\pi \neq \pi'} \frac{\partial \log p(x_t^\pi | y)}{\partial x_0^{\pi'}} \frac{\partial x_0^{\pi'}}{\partial \theta} \right\} \end{aligned} \quad (12)$$

Notice that $\frac{\partial \log p(x_t^\pi | y)}{\partial x_0^{\pi'}}$ = $\nabla_{x_t} \log p(x_t^\pi | y) \frac{\partial x_t^\pi}{\partial x_0^{\pi'}}$ in Eq. (12):

$$\begin{aligned} \nabla_\theta \mathcal{L}_{LD} &= -\mathbb{E}_{\pi, x_t} \left\{ \nabla_{x_t} \log p(x_t^\pi | y) \frac{\partial x_t^\pi}{\partial x_0^\pi} \frac{\partial x_0^\pi}{\partial \theta} \right. \\ &\quad \left. + \sum_{\pi \neq \pi'} \nabla_{x_t} \log p(x_t^\pi | y) \frac{\partial x_t^\pi}{\partial x_0^{\pi'}} \frac{\partial x_0^{\pi'}}{\partial \theta} \right\} \end{aligned} \quad (13)$$

By utilizing the symmetry prior for human heads, we assume that if π and π' are yaw-symmetric camera matrices, $x_t^\pi = \mathbf{M}(x_t^{\pi'})$ where \mathbf{M} is the vertical mirror (flip) operator. Then, by Eq. (1), $\frac{\partial x_t^\pi}{\partial x_0^{\pi'}}$ simply becomes $\mathbf{M}\sqrt{\alpha_t}$. Further simplifying the expression Eq. (13) yields:

$$\nabla_\theta \mathcal{L}_{LD} = -\mathbb{E}_{\pi, x_t} \left\{ \nabla_{x_t} \log p(x_t^\pi | y) \sqrt{\alpha_t} \left(\frac{\partial x_0^\pi}{\partial \theta} + \mathbf{M} \frac{\partial x_0^{\pi'}}{\partial \theta} \right) \right\} \quad (14)$$

As shown in Fig. 2 (a), this intuitively means that we utilize the same score estimation for mirror poses but must also mirror the gradients while back-propagating to the generator. Since 3D-consistent face domain editing with 2D-diffusion models is challenging, keeping the same score estimation for different renders of the same ID under logical constraints avoids deviating from the convergence path. This is because there is no guarantee that $\nabla_{x_t} \log p(x_t^\pi | y)$

and $\nabla_{x_t} \log p(x_t^\pi | y)$ will indicate the same direction for the same y .

Notice the mirror approach can be extended to any render pose tuple (π, π') as long as we can find a tractable gradient chain for $\frac{\partial x_t^\pi}{\partial x_0^\pi}$. Our experiments show that mirror gradients further improve stylization while accentuating 3D-aware features like glasses (Fig. 8).

Multi-view distillation via grid denoising. Mirror gradients only correlate yaw-symmetric poses. Now, let us consider the joint probability distribution p and not assume explicit independence among poses, yielding Eq. (15):

$$q(\theta|y) \propto p(x_0^0, x_0^1, \dots, x_0^N | y) = p(\{x_0^\pi\} | y)$$

$$\nabla_\theta \mathcal{L}_{LD_g} = -\mathbb{E}_{\pi, \{x_t\}} \left\{ \nabla_{\{x_t\}} \log p(\{x_t^\pi\} | y) \frac{\partial \{x_t^\pi\}}{\partial \{x_0^\pi\}} \frac{\partial \{x_0^\pi\}}{\partial \theta} \right\} \quad (15)$$

where $\{x_0^\pi\}$ is defined to have all poses $\{0, 1, \dots, N\}$. However, this is not computationally feasible. Instead, as shown in Fig. 2 (b), we approximate $\{x_0^\pi\}$ with a 2×2 grid, where each element is a x_0^π with different render pose π . This way, denoising UNet can correlate between different renders of θ , improving stylization consistency across views. We further employ a depth-conditioned ControlNet [62] as a regularizer to ensure the estimated score does not collapse to a single fused image.

Our approach does not fine-tune any diffusion model to accommodate multiple inputs [32, 33, 57] for multi-view consistency. Instead, it can use any pre-trained diffusion model and re-purposes grid structures for distillation task, first proposed for video generation [28] and editing [22] with spatiotemporal consistency.

Effect of super-resolution network in style-based 3D GANs. The PanoHead model generates images at a resolution of 512×512 [4], and the diffusion model similarly processes 512×512 images when using LD-losses [47]. For grid construction, we arrange four images in a 2×2 layout but reduce the individual image size to 256×256 to avoid memory issues during forward passes. This way, the final grid image has the size of 512×512 . Although this maintains a good correlation between poses and consistent stylization, it creates a resolution mismatch when gradients are directly propagated from the PanoHead output. To resolve this, we experiment with feeding the gradients before the SR network, where the renderer outputs images at a lower resolution of 64×64 . This adjustment is only necessary for multi-view distillation, where we backpropagate $\nabla_\theta \mathcal{L}_{LD_g}$ before the SR layers. For mirror poses, we do not need to skip the super-resolution layers since they match the correct resolution, and so we backpropagate $\nabla_\theta \mathcal{L}_{LD}$ after the SR, as visualized in Fig. 2. This strategy improves the stylization quality and reduces unwanted artifacts, such as blur, over-saturation, and color tint.

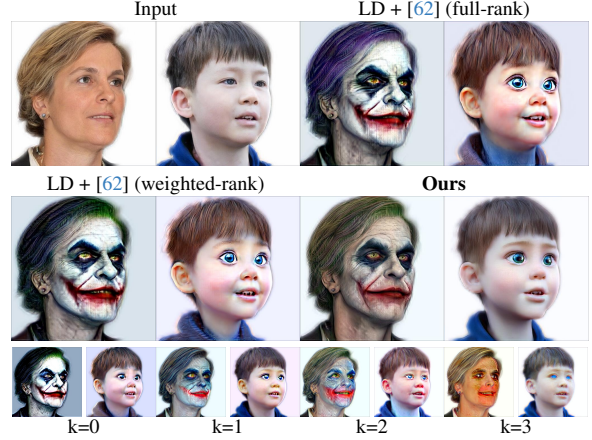


Figure 3. Ablation study on rank weighing. After SVD, four rank-1 matrices are obtained, and k^{th} are chosen for reconstruction. Weighted rank improves the results compared to full rank. In this figure, we also present our final results for comparisons with LD + weighted rank and our multi-view and mirror gradient optimizations for completeness.

4. Experiments

Baselines. We include various domain adaptation methods for our comparisons and adopt all of them for the PanoHead generator. StyleCLIP [40] trains a \mathcal{W}^+ mapper network with the CLIP loss. StyleGAN-NADA [13] employs the CLIP objective to train adaptively-selected generator layers rather than modifying \mathcal{W}^+ . StyleGANFusion [51] utilizes SDS for domain adaptation and a directional regularizer via the frozen generator for more stable distillation. DiffusionGAN3D [29] further improves the regularization of [51] by employing a relative distance loss. After tuning the generators, for inference, we invert images by optimizing \mathcal{W}^+ to reconstruct the input image with the original PanoHead generator. The optimized \mathcal{W}^+ is then fed to these different domain-adapted generators, and rendering from various views is outputted. Details of the baseline implementations are detailed in Supplementary.

Training setup. We train the generator with synthetic $z_{1 \times 512} \sim \mathcal{N}(0, \mathbf{I})$ data for 10k iterations with batch size 1, where the truncation parameter of the generator’s mapping network is $\psi = 0.8$. The optimizer is Adam with a learning rate $1e^{-4}$. The CFG weight and ControlNet guidance weight are set to 7.5 and 1.0, respectively. Depth ground truths are extracted from [55]. More details of the training recipe are provided in Supplementary.

Metrics. For stylization performance, we measure Fréchet Inception Distance (FID) [16] and CLIP embedding similarity; for ID preservation, we measure ArcFace-based [10] ID similarity and multi-view render depth \mathcal{L}_2 difference $\Delta \mathcal{D}$. To construct our test set, we perform \mathcal{W}^+ inversion to randomly chosen ~ 100 FFHQ images. These \mathcal{W}^+ ’s are input



Figure 4. Qualitative stylization results provided in 360-degree views.

to each generator to stylize a real identity.

Specifically, in FID and CLIP, we construct two different edited image distributions, wherein one, the images are edited with a Stable Diffusion pipeline in the 2D image domain (ground-truth distribution), and in the other, the images are edited via the domain-adapted 3D-aware generators. We provide the example images from the ground-truth distribution in Supplementary. We calculate FID between those two image distributions and CLIP scores between paired images.

In ID and $\Delta\mathcal{D}$, we use ground truth unedited images and calculate the scores between the ground-truth original images and stylized images.

Results. We provide quantitative and qualitative results in Tab. 1 and Figs. 1 and 4, respectively. The quantitative results demonstrate that our method outperforms others in terms of stylization quality, as measured by FID and CLIP scores, as well as in identity preservation, as evaluated by ArcFace-based ID similarity and multi-view depth difference $\Delta\mathcal{D}$ across nearly all prompts. These numerical findings are consistent with the visual assessment. As shown in Figs. 1 and 4, StyleCLIP and StyleGAN-NADA produce stylizations of lower quality, with noticeable artifacts in the renderings. While StyleGANFusion and DiffusionGAN3D are capable of producing stylized images, they significantly compromise identity preservation. For instance, in the Joker example in Fig. 1, both methods generate identical facial features for two different identities. Similarly, for the sketch prompt, the identities are substantially altered. Competing methods also remove accessories such as eyeglasses. In

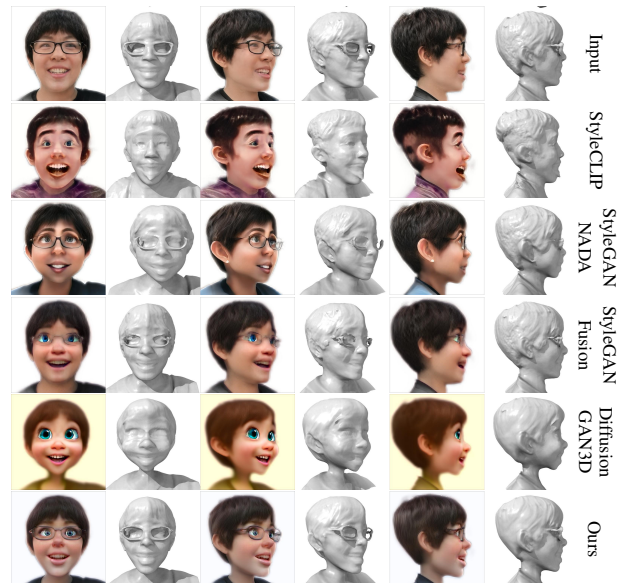


Figure 5. Mesh and rendering visualizations of ours and competing methods for the Pixar prompt. The input consists of a single image, and we display the inverted and rendered results from PanoHead from three different viewpoints.

contrast, our method effectively preserves the identity of the input image while delivering high-quality stylizations.

In Fig. 5, we present the mesh predictions for the Pixar-style stylizations produced by our method and the competing approaches. The first row shows reconstructions of the input image from different views, both in RGB image space

	Pixar				Joker				Werewolf				Sketch				Statue			
	FID	CLIP	ID	$\Delta\mathcal{D}$	FID	CLIP	ID	$\Delta\mathcal{D}$	FID	CLIP	ID	$\Delta\mathcal{D}$	FID	CLIP	ID	$\Delta\mathcal{D}$	FID	CLIP	ID	$\Delta\mathcal{D}$
StyleCLIP [40]	118.2	0.77	0.52	0.022	<u>97.6</u>	0.75	0.38	0.031	248.8	0.63	0.42	0.039	103.7	<u>0.75</u>	<u>0.54</u>	0.026	181.6	0.63	0.61	0.012
StyleGAN-NADA [13]	81.1	0.81	<u>0.61</u>	<u>0.013</u>	116.3	0.81	<u>0.50</u>	0.011	212.9	0.75	0.45	<u>0.012</u>	99.7	0.71	0.51	0.034	154.5	0.76	0.36	0.039
StyleGANFusion [51]	168.0	0.76	0.60	0.003	119.3	0.80	0.41	<u>0.007</u>	203.9	0.70	0.41	<u>0.012</u>	99.0	0.74	0.53	<u>0.012</u>	85.5	0.83	0.47	0.007
DiffusionGAN3D [29]	189.3	<u>0.82</u>	0.46	0.024	110.7	<u>0.86</u>	0.47	0.009	<u>132.3</u>	<u>0.81</u>	0.68	0.002	159.4	0.71	0.48	0.016	166.2	<u>0.82</u>	0.43	<u>0.009</u>
Ours	77.6	0.86	0.69	0.014	67.7	0.89	0.56	0.003	99.7	0.85	<u>0.56</u>	0.002	91.6	0.77	0.75	0.005	<u>144.5</u>	<u>0.82</u>	<u>0.55</u>	0.006

Table 1. Quantitative scores with competitive methods. The first and second best results are shown in **bold** and underlined.

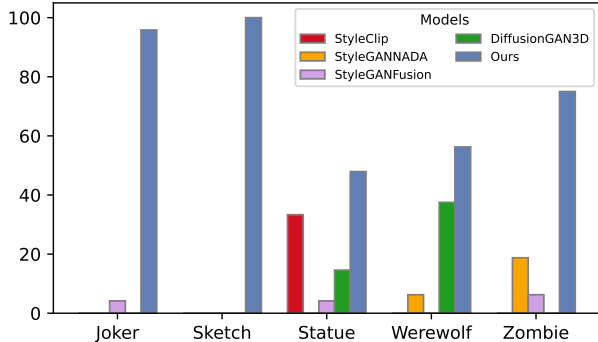


Figure 6. Percentage of users preferences are presented for different prompts. Users overwhelmingly select our method when compared to the other approaches.

and from the mesh perspective. These results demonstrate that our method achieves significantly better identity preservation both in terms of facial features and distinctive accessories, such as eyeglasses. Unlike other methods, which completely remove or distort the eyeglasses, our approach maintains them with high fidelity.

We then conduct a user study with 25 participants to evaluate the quality of 3D stylization and identity preservation across different methods. Participants are shown images generated by five different models: StyleCLIP, StyleGAN-NADA, StyleGANFusion, DiffusionGAN3D, and our own approach. For each image, they are asked to select which output best balances stylization and identity preservation. The methods are presented in random order for each image to minimize bias. Results of this user study are shown in Fig. 6. The data indicate that our method is consistently preferred across all the prompts tested, with participants overwhelmingly selecting it as the best for both stylization and identity preservation when compared to the other approaches.

Ablation Study. We begin our ablation study with the DiffusionGAN3D [29] baseline and build upon it by incorporating various improvements. [29] uses SDS loss for generator optimization, along with a relative distance loss. This relative distance loss aims to preserve the distance between two images generated by the original generator,

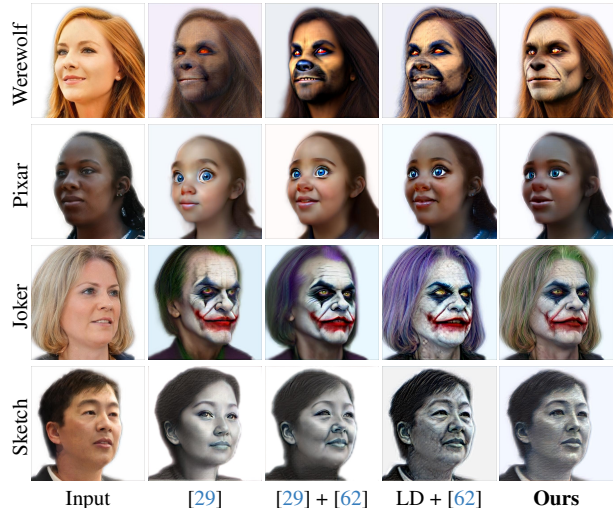


Figure 7. Qualitative Ablation Study I. LD and other regularizers like grid and mirror scores help keep the original hair color, skin tone, and geometry while stylizing.

which serves as the ground truth. The fine-tuned generator is then optimized to maintain this same distance between the corresponding generated samples.

As shown in Fig. 7, while their method successfully achieves stylization, the results fail to preserve the characteristics of the input images. Next, we replace the text-based diffusion model that generates the SDS loss with the depth-based ControlNet [62], which helps retain more characteristics from the input image, though its effectiveness remains limited. In the next setting, we apply negative log-likelihood distillation (LD) alongside the depth-based ControlNet model. This results in less saturation, and we observe improved preservation of the input identity. We also show our final results demonstrating the improved color and geometry alignment with the input images that include the improvements from grid and mirror gradients in the last column. These visuals are consistent with the quantitative improvements presented in Tab. 2.

We continue our ablation study in Fig. 8. We start from the previous study with the results of LD, including rank-weighted score tensors and depth-based ControlNet guidance. The ablation study for rank-weighting is presented

	FID	Δ	CLIP	Δ	ID	Δ
[29]	123.4	-	0.76	-	0.53	-
[29] + [62]	108.3	15.1	0.76	0	0.58	0.05
LD + [62]	93.0	15.3	0.77	0.01	0.76	0.18
LD + [62] + Weighted rank	91.4	1.6	0.76	0.01	0.77	0.01
+ Grid after SR	86.7	4.7	0.79	0.03	0.70	0.07
+ Grid before SR	85.7	1.0	0.79	0	0.72	0.02
+ Mirror gradients	82.3	3.4	0.80	0.01	0.72	0

Table 2. Quantitative ablation study. Δ represents the difference between the results of the current row and the row above it. We use the prompts "sketch", "statue", and "werewolf", and present their averaged results.

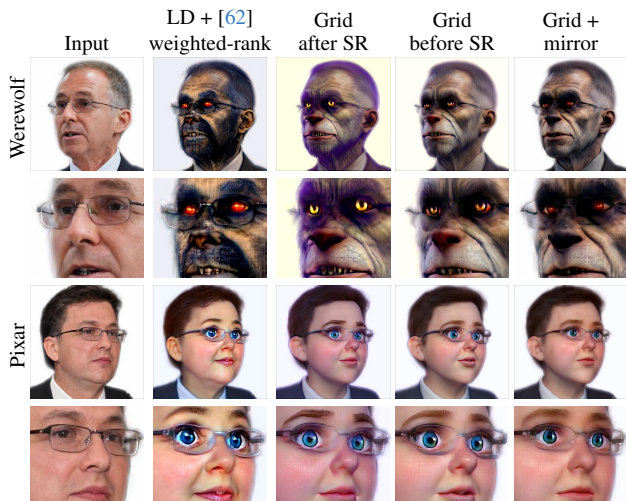


Figure 8. Qualitative Ablation Study II. Grid distillation improves stylization while preserving identity, and mirror gradients focus on symmetric intricate features like glasses.

in Fig. 3 to provide a clearer explanation of the method, so we omit that discussion here. Next, we add the grid-based denoising, which provides multi-view consistent distillation. We observe that the multi-view grid gradients improve the results even when we feed them after the super-resolution layers, but if we feed the gradients to the generator before the super-resolution network, the results improve further both quantitatively and qualitatively, as shown in Tab. 2 and Fig. 8, respectively. Finally, we incorporate cross-dependencies with mirror poses, enhancing intricate details, as evidenced by the zoomed-in views.

Results with other prompts. We present additional results with various prompts in Fig. 9. These prompts include local stylization, such as adding a mustache or editing hair to pink. For these experiments, we do not employ attribute-based masking for score gradients (for example, we do not mask the face when editing the hair). Despite this, our method successfully achieves both localized edits and more



Figure 9. Additional results with various prompts applied to the input image given in the first column.

global transformations, such as modifying the character to resemble an elf under a single framework.

5. Conclusion

We introduced a novel approach to 3D head stylization that improves identity preservation and stylization quality. By utilizing the PanoHead model for 360-degree image synthesis and incorporating negative log-likelihood distillation (LD), mirror and grid score gradients, and score rank weighing, our method overcomes the limitations of previous approaches that struggled with identity retention. Experimental results show significant qualitative and quantitative improvements, advancing the state of 3D head stylization. Our work also provides valuable insights into effective distillation processes between diffusion models and GANs, emphasizing the importance of identity preservation in stylization tasks.

A. LD objective

This section will go through the detailed derivation.

Recall the DDPM forward process:

$$\sqrt{\alpha_t}x_0 + \sqrt{1 - \alpha_t}n = x_t, \quad n \sim \mathcal{N}(0, \mathbf{I}) \quad (16)$$

Assume that distribution (q) of the 3D representation (θ) conditioned on generation prompt (y) is proportional to the prompt-conditioned distribution (p) of independent 2D renders (x_0^i) on different poses (i). In our setup, θ is the style-based 3D GAN layers.

$$q(\theta|y) \propto p(x_0^0, x_0^1, \dots, x_0^N|y) = \prod_i p(x_0^i|y) \quad (17)$$

We optimize negative log-likelihood of Eq. (17) to find θ :

$$-\log q(\theta|y) = -\log \prod_i p(x_0^i|y) = -\sum_i \log p(x_0^i|y) \quad (18)$$

Define the loss \mathcal{L}_{LD} as the average of infinitely many N render poses and find gradient ∇_{θ} to update θ via gradient descent, where π is any given pose:

$$\mathcal{L}_{\text{LD}} = -\frac{1}{N} \lim_{N \rightarrow \infty} \log q(\theta|y) = -\mathbb{E}_{\pi} \{\log p(x_0^{\pi}|y)\} \quad (19)$$

$$\nabla_{\theta} \mathcal{L}_{\text{LD}} = -\mathbb{E}_{\pi} \{\nabla_{\theta} \log p(x_0^{\pi}|y)\}$$

Using Eqs. (16) and (19) and change of variables in probability:

$$p(x_0^{\pi}|y) = p(x_t^{\pi}|y) \left| \frac{\partial x_t}{\partial x_0} \right|^{-1} = \frac{p(x_t^{\pi}|y)}{\sqrt{\alpha_t}} \quad (20)$$

Take the log of both sides, the partial derivative with respect to x_0^{π} , and decompose the right-hand side with chain rule using the relation in Eq. (16):

$$\log p(x_0^{\pi}|y) = \log p(x_t^{\pi}|y) - \log \sqrt{\alpha_t}$$

$$\frac{\partial \log p(x_0^{\pi}|y)}{\partial x_0^{\pi}} = \frac{\partial p(x_t^{\pi}|y)}{\partial x_t^{\pi}} \frac{\partial x_t^{\pi}}{\partial x_0^{\pi}} \quad (21)$$

$$\nabla_{x_0} \log p(x_0^{\pi}|y) = \nabla_{x_t} \log p(x_t^{\pi}|y) \frac{\partial x_t^{\pi}}{\partial x_0^{\pi}}$$

Extend the partial gradient chain in Eq. (21) to θ from x_0^{π} :

$$\nabla_{\theta} \log p(x_0^{\pi}|y) = \nabla_{x_t} \log p(x_t^{\pi}|y) \frac{\partial x_t^{\pi}}{\partial x_0^{\pi}} \frac{\partial x_0^{\pi}}{\partial \theta} \quad (22)$$

where $\nabla_{x_t} \log p(x_t^{\pi}|y)$ is the score function estimation. Plugging Eq. (22) into Eq. (19) yields the update direction:

$$\nabla_{\theta} \mathcal{L}_{\text{LD}} = -\mathbb{E}_{\pi, x_t} \left\{ \nabla_{x_t} \log p(x_t^{\pi}|y) \frac{\partial x_t^{\pi}}{\partial x_0^{\pi}} \frac{\partial x_0^{\pi}}{\partial \theta} \right\} \quad (23)$$

where $\frac{\partial x_t^{\pi}}{\partial x_0^{\pi}}$ is $\sqrt{\alpha_t}$ from Eq. (16). Notice that to update θ , we do not need to back-propagate through denoising UNet and can acknowledge the UNet output as a part of the gradient. Algorithm 1 describes the domain adaptation procedure with PyTorch nomenclature:

Algorithm 1 LD with mirror and grid grads

Require: Generator \mathbf{G}_{θ} , neural renderer \mathbf{R} , super-resolver \mathbf{SR} , depth extractor \mathbf{D} , depth and text-conditioned denoising UNet \mathbf{SD} , generator mapping truncation parameter ψ , extrinsic triplane render matrix π , mirror pose π' , vertical flip operator \mathbf{M} , rank weighing matrix \mathbf{W}

```

1: for  $i$  in  $\{0, 1, \dots, N\}$  do
2:    $w^+ \leftarrow \text{sample\_latent}(\psi=0.8)$ 
3:    $\pi, \pi' \leftarrow \text{sample\_pose}()$   $\triangleright \mathbb{E}_{\pi}$ 
4:    $x_0^{\pi}, x_0^{\pi'} \leftarrow \mathbf{SR}(\mathbf{R}(\mathbf{G}_{\theta}(z), \pi, \pi'))$ 
5:    $n, t \leftarrow \text{noise\_scheduler}(0.70, 0.96)$ 
6:    $x_t^{\pi} \leftarrow \sqrt{\alpha_t}x_0^{\pi} + \sqrt{1 - \alpha_t}n$   $\triangleright \mathbb{E}_{x_t}$ 
7:   with no_grad():
8:      $\nabla_{x_t} \log p(x_t^{\pi}|y) / \sqrt{1 - \alpha_t}$   $\leftarrow$ 
9:      $\mathbf{SD}(x_t^{\pi}, y, t, \mathbf{D}(x_0^{\pi}))$ 
10:    grad  $\leftarrow \nabla_{x_t} \log p(x_t^{\pi}|y) \sqrt{\alpha_t}$ 
11:     $\mathbf{U}\Sigma\mathbf{V}^T \leftarrow \mathbf{SVD}(\text{grad})$ 
12:    grad  $\leftarrow \mathbf{U}\mathbf{W}\Sigma\mathbf{V}^T$   $\triangleright$  rank weighing
13:     $x_0^{\pi'}$ .backward(grad)  $\triangleright \nabla_{\theta} \mathcal{L}_{\text{LD}}$ 
14:    optimizer.step()
15: end for

```

```

16: for  $i$  in  $\{0, 1, \dots, N\}$  do
17:    $w^+ \leftarrow \text{sample\_latent}(\psi=0.8)$ 
18:    $\{\pi\} = \pi^0, \pi^1, \pi^2, \pi^3 \leftarrow \text{sample\_pose}()$   $\triangleright \mathbb{E}_{\{\pi\}}$ 
19:    $\{x_0^{\pi}\}_{\text{LR}} \leftarrow \text{make\_grid}(\mathbf{R}(\mathbf{G}_{\theta}(w^+), \{\pi\}))$ 
20:    $\{x_0^{\pi}\} \leftarrow \text{make\_grid}(\mathbf{SR}(\mathbf{R}(\mathbf{G}_{\theta}(w^+), \{\pi\})))$ 
21:    $n, t \leftarrow \text{noise\_scheduler}(0.30, 0.80)$ 
22:    $\{x_t^{\pi}\} \leftarrow \sqrt{\alpha_t}\{x_0^{\pi}\} + \sqrt{1 - \alpha_t}n$   $\triangleright \mathbb{E}_{\{x_t\}}$ 
23:   with no_grad():
24:      $\nabla_{\{x_t\}} \log p(\{x_t^{\pi}\}|y) / \sqrt{1 - \alpha_t}$   $\leftarrow$ 
25:      $\mathbf{SD}(\{x_t^{\pi}\}, y, t, \mathbf{D}(\{x_0^{\pi}\}))$ 
26:     grad  $\leftarrow \nabla_{\{x_t\}} \log p(\{x_t^{\pi}\}|y) \sqrt{\alpha_t}$ 
27:      $\mathbf{U}\Sigma\mathbf{V}^T \leftarrow \mathbf{SVD}(\text{grad})$ 
28:     grad  $\leftarrow \mathbf{U}\mathbf{W}\Sigma\mathbf{V}^T$   $\triangleright$  rank weighing
29:      $\{x_0^{\pi}\}_{\text{LR}}$ .backward(grad)  $\triangleright$  grid gradients  $\nabla_{\theta} \mathcal{L}_{\text{LD}_g}$ 
30:     optimizer.step()
31: end for

```

31: return \mathbf{G}_{θ}

`sample_latent` utilizes the mapping network of the generator and maps z to w^+ , later to be fed to the generator. `make_grid` creates a 2×2 grid with 4 inputs. \mathbf{M} is realized with `torch.flip(x, dims=[-1])`. `with no_grad()` disables PyTorch's gradient calculation. Note that each time x_0 is generated, we implicitly pass it through VQ-VAE to embed it into \mathbf{SD} 's latent space.

B. Implementation details

Baselines. We train the latent mapper in StyleCLIP [40] with PanoHead’s [4] generator. For StyleGAN-NADA [13] and StyleGANFusion [51], we use [51]’s official repository and modify the generator backbone to PanoHead. For [51], we utilize their EG3D config parameters for PanoHead, and implement the adaptive layer selection for [13]. For DiffusionGAN3D [29], we implement the method based on the official paper since there is no published codebase. For our baseline, we utilize our implementation of [29] with their distance loss for domain adaptation and build upon it with our proposed improvements. We stay faithful to each baseline’s original hyperparameters (denoiser checkpoint selection, noise scheduler, learning rate, optimizer, etc.) unless the training diverges.

Our training parameters. We train the generator with synthetic $z_{1 \times 512} \sim \mathcal{N}(0, \mathbf{I})$ data for 10k iterations with batch size 1, where the truncation parameter of the generator’s mapping network is $\psi = 0.8$. We use Adam optimizer with a $1e^{-4}$ learning rate. We optimize the `G.backbone.synthesis` and `G.backbone.superresolution` sub-networks of the generator `G` and freeze all convolutional layer biases, using the same configuration as [51]. The classifier-free-guidance (CFG) [18] weight and depth-conditioned ControlNet [62]¹ guidance weight are set to 7.5 and 1.0, respectively. Depth ground truths are extracted from [55] since the neural renderer’s depth estimations are low-resolution and require additional clipping (64×64).

As the conditional denoiser for our method and the ablation study for showing the improvements upon [29], we employ RV v5.1². For qualitative and quantitative comparison among other methods, we employ the methods’ suggested diffusion checkpoints in their papers and repositories^{3,4}.

For mirror and grid denoising, noise start timestep t is uniformly selected among $(0.70, 0.96)$ and $(0.30, 0.80)$, respectively, where t is from $0 \rightarrow 1$. We use `DDIMScheduler` for the noise scheduler. The number of inference steps in the diffusion pipeline is always 1 since we perform score distillation.

Quantitative scores. We construct ground-truth edited image distributions using the Stable Diffusion pipeline. For the first distribution, we take images, add noise with $t = 25$, and denoise with the style prompt using each baseline’s diffusion checkpoints for 50 steps, resulting in edited images.



Figure 10. From left to right: Ours (distribution #2), ground truth unedited image (distribution #3), edited image with full-step diffusion pipeline (distribution #1).

The second distribution consists of the same images stylized using domain-adapted generators. These two distributions are used to compute FID, and individual image pairs between them are used to compute CLIP similarity scores. We generate a third distribution using unedited images to evaluate identity preservation (ID) and $\Delta\mathcal{D}$. Scores for ID and $\Delta\mathcal{D}$ are then calculated between using image pairs from the second and third distributions. Fig. 10 visualizes sample images in those three distributions.

Prompts. We use empty strings for negative prompts for our method. For positive prompts, we use the following list for all methods:

- Portrait a person in Pixar style, cute, big eyes, Disney, sharp, 8K, skin detail, best quality, realistic lighting, good-looking, uniform light, extremely detailed
- Portrait of a Greek statue, closeup, elegant and timeless, intricate and detailed carving, smooth marble texture, ancient Greek aesthetics
- A portrait of Joker from the movie The Dark Knight
- Charcoal pencil sketch of human face, lower third, high contrast, black and white
- Portrait of a werewolf
- Portrait of a zombie

¹<https://huggingface.co/llyasviel/sd-controlnet-depth>

²https://huggingface.co/SG161222/Realistic_Vision_V5.1_noVAE

³<https://huggingface.co/stable-diffusion-v1-5/stable-diffusion-v1-5>

⁴<https://huggingface.co/stabilityai/stable-diffusion-2>

References

- [1] Rameen Abdal, Hsin-Ying Lee, Peihao Zhu, Menglei Chai, Aliaksandr Siarohin, Peter Wonka, and Sergey Tulyakov. 3davatar: Bridging domains for personalized editable avatars. In *Proceedings of the IEEE/CVF Conference on Computer Vision and Pattern Recognition*, pages 4552–4562, 2023. [2](#)
- [2] Rameen Abdal, Yipeng Qin, and Peter Wonka. Image2stylegan: How to embed images into the stylegan latent space? In *Proceedings of the IEEE/CVF International Conference on Computer Vision*, pages 4432–4441, 2019. [2](#)
- [3] Yuval Alaluf, Omer Tov, Ron Mokady, Rinon Gal, and Amit Bermano. Hyperstyle: Stylegan inversion with hypernetworks for real image editing. In *Proceedings of the IEEE/CVF Conference on Computer Vision and Pattern Recognition*, pages 18511–18521, 2022. [2](#)
- [4] Sizhe An, Hongyi Xu, Yichun Shi, Guoxian Song, Umit Y Ogras, and Linjie Luo. Panohead: Geometry-aware 3d full-head synthesis in 360deg. In *Proceedings of the IEEE/CVF conference on computer vision and pattern recognition*, pages 20950–20959, 2023. [2](#), [3](#), [5](#), [10](#)
- [5] Qingyan Bai, Zifan Shi, Yinghao Xu, Hao Ouyang, Qiuyu Wang, Ceyuan Yang, Xuan Wang, Gordon Wetzstein, Yujun Shen, and Qifeng Chen. Real-time 3d-aware portrait editing from a single image. In *ECCV*, 2024. [2](#)
- [6] Ananta R Bhattarai, Matthias Nießner, and Artem Sevastopolsky. Triplanenet: An encoder for eg3d inversion. In *Proceedings of the IEEE/CVF Winter Conference on Applications of Computer Vision*, pages 3055–3065, 2024. [2](#)
- [7] Bahri Batuhan Bilecen, Ahmet Berke Gokmen, and Aysegul Dundar. Dual encoder gan inversion for high-fidelity 3d head reconstruction from single images. In *Advances in Neural Information Processing Systems (NeurIPS)*, 2024. [2](#)
- [8] Eric R Chan, Connor Z Lin, Matthew A Chan, Koki Nagano, Boxiao Pan, Shalini De Mello, Orazio Gallo, Leonidas J Guibas, Jonathan Tremblay, Sameh Khamis, et al. Efficient geometry-aware 3d generative adversarial networks. In *Proceedings of the IEEE/CVF conference on computer vision and pattern recognition*, pages 16123–16133, 2022. [2](#)
- [9] Eric R Chan, Marco Monteiro, Petr Kellnhofer, Jiajun Wu, and Gordon Wetzstein. pi-gan: Periodic implicit generative adversarial networks for 3d-aware image synthesis. In *Proceedings of the IEEE/CVF conference on computer vision and pattern recognition*, pages 5799–5809, 2021. [2](#)
- [10] Jiankang Deng, Jia Guo, Niannan Xue, and Stefanos Zafeiriou. Arcface: Additive angular margin loss for deep face recognition. In *Proceedings of the IEEE/CVF Conference on Computer Vision and Pattern Recognition*, pages 4690–4699, 2019. [5](#)
- [11] Aysegul Dundar, Jun Gao, Andrew Tao, and Bryan Catanzaro. Fine detailed texture learning for 3d meshes with generative models. *IEEE Transactions on Pattern Analysis and Machine Intelligence*, 2023. [2](#)
- [12] Aysegul Dundar, Jun Gao, Andrew Tao, and Bryan Catanzaro. Progressive learning of 3d reconstruction network from 2d gan data. *IEEE Transactions on Pattern Analysis and Machine Intelligence*, 2023. [2](#)
- [13] Rinon Gal, Or Patashnik, Haggai Maron, Amit H Bermano, Gal Chechik, and Daniel Cohen-Or. Stylegan-nada: Clip-guided domain adaptation of image generators. *ACM Transactions on Graphics (TOG)*, 41(4):1–13, 2022. [2](#), [5](#), [7](#), [10](#)
- [14] Jiatao Gu, Lingjie Liu, Peng Wang, and Christian Theobalt. Stylenerf: A style-based 3d-aware generator for high-resolution image synthesis. *arXiv preprint arXiv:2110.08985*, 2021. [2](#)
- [15] Paul Henderson, Vagia Tsiminaki, and Christoph H Lampert. Leveraging 2d data to learn textured 3d mesh generation. In *Proceedings of the IEEE/CVF conference on computer vision and pattern recognition*, pages 7498–7507, 2020. [2](#)
- [16] Martin Heusel, Hubert Ramsauer, Thomas Unterthiner, Bernhard Nessler, and Sepp Hochreiter. Gans trained by a two time-scale update rule converge to a local nash equilibrium. *Advances in neural information processing systems*, 30, 2017. [5](#)
- [17] Jonathan Ho, Ajay Jain, and Pieter Abbeel. Denoising diffusion probabilistic models. In *Advances in Neural Information Processing Systems*, volume 33, pages 6840–6851. Curran Associates, Inc., 2020. [3](#)
- [18] Jonathan Ho and Tim Salimans. Classifier-free diffusion guidance, 2022. [4](#), [10](#)
- [19] Fangzhou Hong, Mingyuan Zhang, Liang Pan, Zhongang Cai, Lei Yang, and Ziwei Liu. Avatarclip: Zero-shot text-driven generation and animation of 3d avatars. *arXiv preprint arXiv:2205.08535*, 2022. [3](#)
- [20] Shuo Huang, Shikun Sun, Zixuan Wang, Xiaoyu Qin, Yanmin Xiong, Yuan Zhang, Pengfei Wan, Di Zhang, and Jia Jia. Placiddreamer: Advancing harmony in text-to-3d generation, 2024. [2](#), [3](#), [4](#)
- [21] Erik Härkönen, Aaron Hertzmann, Jaakko Lehtinen, and Sylvain Paris. Ganspace: Discovering interpretable gan controls. In *Advances in Neural Information Processing Systems (NeurIPS)*, 2020. [4](#)
- [22] Ozgur Kara, Bariscan Kurtkaya, Hidir Yesiltepe, James M. Rehg, and Pinar Yanardag. Rave: Randomized noise shuffling for fast and consistent video editing with diffusion models. In *Proceedings of the IEEE/CVF Conference on Computer Vision and Pattern Recognition*, 2024. [5](#)
- [23] Tero Karras, Samuli Laine, and Timo Aila. A style-based generator architecture for generative adversarial networks. In *Proceedings of the IEEE/CVF Conference on Computer Vision and Pattern Recognition*, pages 4401–4410, 2019. [2](#)
- [24] Tero Karras, Samuli Laine, Miika Aittala, Janne Hellsten, Jaakko Lehtinen, and Timo Aila. Analyzing and improving the image quality of stylegan. In *Proceedings of the IEEE/CVF conference on computer vision and pattern recognition*, pages 8110–8119, 2020. [2](#)
- [25] Gwanghyun Kim and Se Young Chun. Datid-3d: Diversity-preserved domain adaptation using text-to-image diffusion for 3d generative model. In *Proceedings of the IEEE/CVF conference on computer vision and pattern recognition*, pages 14203–14213, 2023. [2](#)
- [26] Gwanghyun Kim, Ji Ha Jang, and Se Young Chun. Podia-3d: Domain adaptation of 3d generative model across large domain gap using pose-preserved text-to-image diffusion. In *Proceedings of the IEEE/CVF international conference on computer vision*, pages 22603–22612, 2023. [2](#)
- [27] Sehyung Lee, Mijung Kim, Yeongnam Chae, and Björn

- Stenger. Linearly controllable gan: Unsupervised feature categorization and decomposition for image generation and manipulation. In *Computer Vision – ECCV 2024*, pages 229–245. Springer Nature Switzerland, 2025. 4
- [28] Taegyeong Lee, Soyeong Kwon, and Taehwan Kim. Grid diffusion models for text-to-video generation. In *Proceedings of the IEEE/CVF Conference on Computer Vision and Pattern Recognition*, pages 8734–8743, 2024. 5
- [29] Biwen Lei, Kai Yu, Mengyang Feng, Miaomiao Cui, and Xuansong Xie. Diffusiongan3d: Boosting text-guided 3d generation and domain adaption by combining 3d gans and diffusion priors. In *CVPR*, 2024. 2, 3, 5, 7, 8, 10
- [30] Xueting Li, Shalini De Mello, Sifei Liu, Koki Nagano, Umar Iqbal, and Jan Kautz. Generalizable one-shot 3d neural head avatar. *Advances in Neural Information Processing Systems*, 36, 2024. 2
- [31] Bingchen Liu, Yizhe Zhu, Kunpeng Song, and Ahmed Elgammal. Towards faster and stabilized gan training for high-fidelity few-shot image synthesis. In *International conference on learning representations*, 2020. 2
- [32] Ruoshi Liu, Rundi Wu, Basile Van Hoorick, Pavel Tokmakov, Sergey Zakharov, and Carl Vondrick. Zero-1-to-3: Zero-shot one image to 3d object. In *Proceedings of the IEEE/CVF International Conference on Computer Vision (ICCV)*, pages 9298–9309, October 2023. 5
- [33] Yuan Liu, Cheng Lin, Zijiao Zeng, Xiaoxiao Long, Lingjie Liu, Taku Komura, and Wenping Wang. Syncdreamer: Generating multiview-consistent images from a single-view image. In *ICLR*, 2024. 5
- [34] Ben Mildenhall, Pratul P Srinivasan, Matthew Tancik, Jonathan T Barron, Ravi Ramamoorthi, and Ren Ng. Nerf: Representing scenes as neural radiance fields for view synthesis. *Communications of the ACM*, 65(1):99–106, 2021. 2
- [35] Nasir Mohammad Khalid, Tianhao Xie, Eugene Belilovsky, and Tiberiu Popa. Clip-mesh: Generating textured meshes from text using pretrained image-text models. In *SIGGRAPH Asia 2022 conference papers*, pages 1–8, 2022. 3
- [36] Michael Niemeyer and Andreas Geiger. Giraffe: Representing scenes as compositional generative neural feature fields. In *Proceedings of the IEEE/CVF Conference on Computer Vision and Pattern Recognition*, pages 11453–11464, 2021. 2
- [37] Utkarsh Ojha, Yijun Li, Jingwan Lu, Alexei A Efros, Yong Jae Lee, Eli Shechtman, and Richard Zhang. Few-shot image generation via cross-domain correspondence. In *Proceedings of the IEEE/CVF conference on computer vision and pattern recognition*, pages 10743–10752, 2021. 2
- [38] OpenAI. Dall-e 3: A system for generating images from text prompts, 2023. 3
- [39] Roy Or-El, Xuan Luo, Mengyi Shan, Eli Shechtman, Jeong Joon Park, and Ira Kemelmacher-Shlizerman. Stylesdf: High-resolution 3d-consistent image and geometry generation. In *Proceedings of the IEEE/CVF Conference on Computer Vision and Pattern Recognition*, pages 13503–13513, 2022. 2
- [40] Or Patashnik, Zongze Wu, Eli Shechtman, Daniel Cohen-Or, and Dani Lischinski. Styleclip: Text-driven manipulation of stylegan imagery. In *ICCV*, October 2021. 2, 5, 7, 10
- [41] Dario Pavllo, Graham Spinks, Thomas Hofmann, Marie-Francine Moens, and Aurelien Lucchi. Convolutional generation of textured 3d meshes. *Advances in Neural Information Processing Systems*, 33:870–882, 2020. 2
- [42] Hamza Pehlivan, Yusuf Dalva, and Aysegül Dundar. Styleres: Transforming the residuals for real image editing with stylegan. In *Proceedings of the IEEE/CVF Conference on Computer Vision and Pattern Recognition*, pages 1828–1837, 2023. 2
- [43] Justin NM Pinkney and Doron Adler. Resolution dependent gan interpolation for controllable image synthesis between domains. *arXiv preprint arXiv:2010.05334*, 2020. 2
- [44] Dustin Podell, Zion English, Kyle Lacey, Andreas Blattmann, Tim Dockhorn, Jonas Müller, Joe Penna, and Robin Rombach. Sdxl: Improving latent diffusion models for high-resolution image synthesis. *arXiv preprint arXiv:2307.01952*, 2023. 3
- [45] Ben Poole, Ajay Jain, Jonathan T. Barron, and Ben Mildenhall. Dreamfusion: Text-to-3d using 2d diffusion. In *ICLR*, 2023. 2, 3, 4
- [46] Daniel Roich, Ron Mokady, Amit H Bermano, and Daniel Cohen-Or. Pivotal tuning for latent-based editing of real images. *ACM Transactions on Graphics (TOG)*, 42(1):1–13, 2022. 2
- [47] Robin Rombach, Andreas Blattmann, Dominik Lorenz, Patrick Esser, and Björn Ommer. High-resolution image synthesis with latent diffusion models. In *Proceedings of the IEEE/CVF Conference on Computer Vision and Pattern Recognition (CVPR)*, pages 10684–10695, June 2022. 3, 5
- [48] Chitwan Saharia, William Chan, Saurabh Saxena, Lala Li, Jay Whang, Emily L Denton, Kamyar Ghasemipour, Raphael Gontijo Lopes, Burcu Karagol Ayan, Tim Salimans, et al. Photorealistic text-to-image diffusion models with deep language understanding. *Advances in neural information processing systems*, 35:36479–36494, 2022. 3
- [49] Aditya Sanghi, Hang Chu, Joseph G Lambourne, Ye Wang, Chin-Yi Cheng, Marco Fumero, and Kamal Rahimi Malekshah. Clip-forge: Towards zero-shot text-to-shape generation. In *Proceedings of the IEEE/CVF Conference on Computer Vision and Pattern Recognition*, pages 18603–18613, 2022. 3
- [50] Guoxian Song, Hongyi Xu, Jing Liu, Tiancheng Zhi, Yichun Shi, Jianfeng Zhang, Zihang Jiang, Jiashi Feng, Shen Sang, and Linjie Luo. Agilegan3d: Few-shot 3d portrait stylization by augmented transfer learning. In *Proceedings of the IEEE/CVF Conference on Computer Vision and Pattern Recognition*, pages 765–774, 2024. 2
- [51] Kunpeng Song, Ligong Han, Bingchen Liu, Dimitris Metaxas, and Ahmed Elgammal. Diffusion guided domain adaptation of image generators. In *WACV*, 2024. 2, 3, 5, 7, 10
- [52] Yang Song, Jascha Sohl-Dickstein, Diederik P Kingma, Abhishek Kumar, Stefano Ermon, and Ben Poole. Score-based generative modeling through stochastic differential equations. In *International Conference on Learning Representations*, 2021. 3
- [53] Zhengyi Wang, Cheng Lu, Yikai Wang, Fan Bao, Chongxuan Li, Hang Su, and Jun Zhu. Prolificdreamer: High-fidelity and diverse text-to-3d generation with variational score distilla-

- tion. In *Advances in Neural Information Processing Systems (NeurIPS)*, 2023. 4
- [54] Jiaxin Xie, Hao Ouyang, Jingtian Piao, Chenyang Lei, and Qifeng Chen. High-fidelity 3d gan inversion by pseudo-multi-view optimization. In *Proceedings of the IEEE/CVF Conference on Computer Vision and Pattern Recognition*, pages 321–331, 2023. 2
- [55] Lihe Yang, Bingyi Kang, Zilong Huang, Zhen Zhao, Xiaogang Xu, Jiashi Feng, and Hengshuang Zhao. Depth anything v2. *Advances in Neural Information Processing Systems (NeurIPS)*, 2024. 5, 10
- [56] Shuai Yang, Liming Jiang, Ziwei Liu, and Chen Change Loy. Pastiche master: Exemplar-based high-resolution portrait style transfer. In *Proceedings of the IEEE/CVF Conference on Computer Vision and Pattern Recognition*, pages 7693–7702, 2022. 2
- [57] Yunhan Yang, Yukun Huang, Xiaoyang Wu, Yuan-Chen Guo, Song-Hai Zhang, Hengshuang Zhao, Tong He, and Xihui Liu. Dreamcomposer: Controllable 3d object generation via multi-view conditions. In *CVPR*, 2024. 5
- [58] Ahmet Burak Yildirim, Hamza Pehlivan, Bahri Batuhan Bilecen, and Aysegul Dundar. Diverse inpainting and editing with gan inversion. In *Proceedings of the IEEE/CVF International Conference on Computer Vision*, pages 23120–23130, 2023. 2
- [59] Ahmet Burak Yildirim, Hamza Pehlivan, and Aysegul Dundar. Warping the residuals for image editing with stylegan. *International Journal of Computer Vision*, pages 1–16, 2024. 2
- [60] Ziyang Yuan, Yiming Zhu, Yu Li, Hongyu Liu, and Chun Yuan. Make encoder great again in 3d gan inversion through geometry and occlusion-aware encoding. In *Proceedings of the IEEE/CVF international conference on computer vision*, 2023. 2
- [61] Junzhe Zhang, Yushi Lan, Shuai Yang, Fangzhou Hong, Quan Wang, Chai Kiat Yeo, Ziwei Liu, and Chen Change Loy. Deformtoon3d: Deformable neural radiance fields for 3d toonification. In *Proceedings of the IEEE/CVF International Conference on Computer Vision*, pages 9144–9154, 2023. 2
- [62] Lvmin Zhang, Anyi Rao, and Maneesh Agrawala. Adding conditional control to text-to-image diffusion models. In *Proceedings of the IEEE/CVF International Conference on Computer Vision (ICCV)*, pages 3836–3847, October 2023. 5, 7, 8, 10